metals

MDPI

Article

Superconductivity in the Intercalated Graphite Compound CaC_6 and the Roeser–Huber Formalism

Michael R. Koblischka [1,2,*] and Anjela Koblischka-Veneva [1,2]

[1] Saarland University, P.O. Box 151150, 66041 Saarbrücken, Germany; a.koblischka@gmail.com
[2] SupraSaar, 66133 Saarbrücken-Scheidt, Germany
* Correspondence: m.koblischka@gmail.com or m.koblischka@ieee.org

Abstract

The superconducting transition temperature, T_c, of the graphite intercalation compound, CaC_6, was calculated using the Roeser–Huber (RH) formalism. This method was adapted to alloys with complex crystal structures by identifying symmetric paths for the superconducting charge carriers (Cooper pairs) and incorporating interactions with neighboring atoms through phonon coupling. The evaluation of the lowest energy levels, $\Delta_{(0)}$, along all relevant crystallographic directions reveals a slight anisotropy between the in-plane and out-of-plane directions, consistent with the experimental observation of the gap anisotropy by point contact spectroscopy. The T_c values obtained for CaC_6, CaC_6 with applied high pressure, and YbC_6 show good agreement with experimental data, thereby supporting both the validity of the RH approach and its predictive capability in describing superconductivity within complex crystal structures.

Keywords: Graphite intercalation compounds; CaC_6; YbC_6; graphene; superconducting transition; T_c; Roeser-Huber formalism; superconducting paths

Academic Editor: Jiro Kitagawa

Received: 19 October 2025
Revised: 2 December 2025
Accepted: 7 December 2025
Published: 11 December 2025

Citation: Koblischka, M.R.; Koblischka-Veneva, A. Superconductivity in the Intercalated Graphite Compound CaC_6 and the Roeser–Huber Formalism. *Metals* **2025**, *15*, 1367. https://doi.org/10.3390/met15121367

1. Introduction

The graphite intercalation compound (GIC) CaC_6 represents a remarkable superconducting material with a relatively high superconducting transition temperature, T_c, of about 11.6 K [1–5] discovered in 2005. The recorded T_c is strikingly higher than those of previously known GICs, which exhibited transition temperatures up to only 4.05 K (see, e.g., Refs. [6,7]). CaC_6 can be viewed either as a graphite structure with intercalated calcium atoms or as a two-dimensional graphene layer embedded within a calcium unit cell. Consequently, the crystal structure contains a relatively large number of atoms per unit cell. Another GIC, YbC_6, exhibiting T_c ∼6 K, was also reported in Ref. [1], though it possesses a different crystal structure. This material will be discussed in detail in the Supplementary Materials.

The 2D graphene layer can be considered as model system of a two-dimensional electron gas, the electronic properties of which can be altered through intercalation. The finding of the quite high T_c triggered several theoretical works to investigate the physical and superconducting properties [8–10], as well as experimental work investigating mutual inductance measurements [11], point-contact spectroscopy [12] or scanning tunneling microscopy/spectroscopy (STM/STS) [13,14], and the application of pressure. Application of high pressure was found to increase T_c up to 15.1 K at 7.5 GPa [15–17], followed by a drop to T_c ∼5 K at 8 GPa [17].

All these features make the CaC_6 superconductor an interesting target to check out the principles of the Roeser–Huber (RH) formalism to calculate T_c solely based on the

electronic properties and the given crystal structure with no free parameters, as shown previously in Refs. [18–21]. The goal of the RH formalism is to find a superconducting path within the crystal unit cell that can accommodate a superconducting charge carrier wave. Thus, we must note here that the RH formalism does not contain any means to calculate the pairing interaction. This is left for ab initio calculations. It is, however, important to point out that the present RH formalism fulfills the longstanding dream [22] to establish a relation between a given crystallographic structure and the resulting superconductivity.

The RH approach has already been successfully applied to the case of magic-angle twisted bilayer graphene (MATBG) [23], a pure graphene system without doping. The presence of graphene layers within CaC_6 thus provides an excellent test for the RH concepts of symmetric charge carrier paths and "passed atoms," which influence the superconducting carrier wave through phonon interactions.

For a meaningful application of the RH formalism, knowledge of a well-defined crystal structure is essential. The work of Emery et al. [2–4] who developed a efficient synthesis method of bulk CaC_6 provided this foundation. CaC_6 crystallizes in a rhombohedral structure (space group $R\bar{3}m$), with the elemental unit cell containing one Ca atom and six carbon atoms. This makes the CaC_6 unique among the binary GIC materials, which commonly exhibit a hexagonal symmetry. A figure of the crystal structure is presented in Section 3.1 below.

The present manuscript is organized as follows: In Section 2, the details of the Roeser–Huber formalism required for the T_c calculation of alloys and compounds are laid out. Section 3 presents the crystal structure, the electronic configuration and the calculation steps required for the graphite intercalation compound, CaC_6. Furthermore, the findings are discussed. Finally, Section 4 presents our conclusions. Additionally, the Supplementary Materials shows the crystal structure and the calculations for YbC_6.

2. Roeser–Huber Formalism for Alloys

A detailed discussion of the Roeser–Huber (RH) formalism, as applied to various elements and alloys, has been presented previously in Refs. [20,21]. Therefore, we summarize here only the most relevant steps and provide a graphical overview in Figure 1.

Superconductivity in the RH formalism is seen as a resonance effect between the charge carrier wave formed by Cooper pairs with the de Broglie wavelength, λ_{cc}, of the superconducting charge carriers that moves through the crystal lattice. A characteristic distance, x, within the given crystal unit cell determines the path for the charge carriers. This picture can be straightforwardly understood when interpreting the superconducting transition seen in a resistance measurement as an integrated resonance curve. The underlying physics is given by the particle-in-box (PiB) principle of quantum mechanics [24].

The complete Roeser–Huber formula is formulated as described in Refs. [19–21]:

$$\Delta_{(0)\mathrm{ges}} = \frac{h^2}{2M_\mathrm{L}} \cdot \left(\sum_{i=1}^{n} \frac{1}{(2x_{R_i})^2} \cdot n_0^{2/3} \cdot \frac{n_{2R_i}}{n_{1R_i}} \right) = \pi k_B T_{c(0)}, \tag{1}$$

where

(1) $\Delta_{(0)}$ represents the lowest energy level of the PiB.
(2) h is the Planck constant.
(3) M_L represents a parameter with the unit of a mass.
(3) n_0 indicates the number of superconducting planes in the case of 2D superconductors, and will be set here to $n_0 = 1$.
(4) n_1 and n_2 are two important factors to describe the crystallographic environment of each possible path as described below.

(5) The index R_i indicates all possible superconducting paths within the crystal lattice.
(6) k_B is the Boltzmann constant.

For each crystallographic direction R_i (to be called the superconducting path hereafter), the two factors, n_1 and n_2, must be determined to obtain a complete picture for the calculation of $T_{c(0)}$.

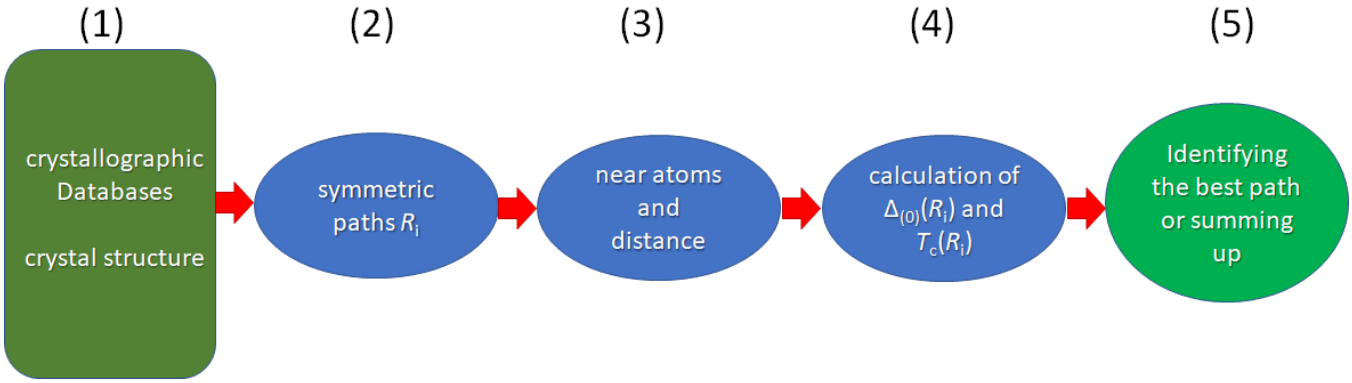

Figure 1. A schematic illustration of the steps required in the RH formalism to obtain the data required for the calculation of the superconducting transition temperature, T_c.

In the seminal work of Stepper [19], who calculated T_c of several two-component alloys, three essential points were formulated, all of which must be properly treated when calculating T_c for alloys and compounds. As this work is an unpublished graduation work, these points are fundamental and are summarized below:

(i) The characteristic distance x_{R_i} can be obtained only from *symmetric* paths (in the following, these will be called superconducting paths), along which the charge carrier wave propagates through the crystal lattice. Path symmetry is essential: any asymmetry introduces phase disruption due to uneven forces acting on the carriers. Thus, most directions are excluded from consideration.
(ii) The factor n_1 accounts for atoms located near the superconducting path, which influence the carriers via phonon interaction. Therefore, it is essential to determine the distance of these atoms to the respective superconducting path and to count the number of atoms passed within a unit cell. All atoms fulfilling the relation $l/x \leq 0.5$ with l describing the distance of the atom to the selected superconducting path, i.e., to the moving charge carrier wave, are then counted as N_{atoms}. The parameter n_1 is then calculated via the relation $n_1 = N_L/N_{\text{atoms}}$, where N_L denotes the number of the charge carriers.
(iii) A second factor, n_2, is introduced to describe the relationship among the various possible paths of the charge carrier wave, R_i, within a given crystal structure. Such a factor becomes necessary in complex structures where multiple superconducting paths coexist and are carried by different atomic species, as observed in compounds such as MgB_2 or the A15-type superconductors, which were already discussed in Ref. [20]. In this context, n_2 characterizes the relation between equivalent paths oriented along the same crystallographic direction. For the systems considered in this work, no such multiplicity of paths is present; therefore for CaC_6, $n_2 = 1$.

It should be noted that the superconducting pairing interaction may involve multiple phonon modes (vibrational modes of the lattice), each contributing differently to the overall electron–phonon coupling constant. This behavior is characteristic of complex crystal structures such as the GICs and A15-type superconductors, where several optical and acoustic phonon branches interact with conduction electrons. In the RH framework, this

multimode phonon coupling is effectively captured through the counting of the near, passed atoms along a given superconducting path.

As consequence of the above, the energy $\Delta_{(0)}$ and the corresponding $T_{c(0)}$ must be calculated for each of the existing superconducting paths, R_i, and the results may then be summed up following Equation (1) to obtain the T_c for a given crystal structure.

All the points (i)–(iii) give, together with Equation (1), the full Roeser–Huber formalism for metals and alloys. It is important to point out here that this formalism does not contain any free parameters, as all the required inputs are given via the crystal unit cell (i.e., the characteristic length x and N_{atoms}) and N_L from the basic electronic configuration of the material. Another important issue is that the Roeser–Huber formalism does not include any means how the Cooper pairs are formed, so we cannot predict if a given material is a superconductor.

To obtain the data for the parameter M_{L}, in the original works of RH [18,19] the mass of a proton, m_p, was employed, even though the charge carriers involved are Cooper pairs with the mass 2 m_e, the electron mass. This choice is justified by the RH plot (see Refs. [20,23]), where a scaling factor of 1903.6 aligns the data for metals, alloys and high-temperature superconductors along a single line with a slope $h^2/(2\pi k_B) = 5.061 \times 10^{-45}$ m^2 kg K. Thus, this factor reflects the different Fermi temperatures [25] for the various materials. Now, the quotient of m_p/m_e yields 1836.15, which is quite close to 1903.6 (i.e., 3.5% error), which justified the use of m_p in the calculations. As discussed in Ref. [23], it is better to write here $M_L = \eta 2m_e$ for a Cooper pair. For alloys, η will be higher according to the different Fermi temperatures as compared to the HTSc, leading here to a value of $\eta = 918.1$ (that is, $m_p/(2m_e)$).

The required crystallographic data come from respective databases [26–28], enabling the RH formalism to be integrated into machine learning frameworks for predictive superconductivity studies [29–32].

3. Results and Discussion

3.1. Crystal Strucure of CaC_6

CaC_6 is the only member of the GIC with a rhombohedral unit cell (space group R$\bar{3}$m) with the lattice parameters $a = b = 0.517$ nm, $\alpha = 49.55°$. For convenience, however, rhombohedral crystals are often represented using a hexagonal unit cell that is three times larger in volume. In this description, the lattice parameters are $a = 0.4333$ nm and $c = 1.3572$ nm. Since the interlayer spacing between carbon sheets is $d = 0.4524$ nm, we obtain $c = 3d = 1.3572$ nm. In this representation, the shortest Ca–Ca distance in the intercalant layer is $a = 0.4333$ nm, and the closest C–C distance is $d_{CC} = 0.1444$ nm. The Wyckhof positions for this hexagonal structure were determined in Ref. [2] are as follows:

Carbon: 18 atoms 18g (1/3 0 1/2);
Calcium: 3 atoms 3a (0 0 0).

With this information, the unit cell can be drawn using CrystalMaker V11 [33] or VESTA V3.9 [34] software. In this work, we adopt the hexagonal unit cell for CaC_6 (Figure 2a) because it also facilitates applying the superconducting path selection procedure also YbC_6, as discussed in the Supplementary Materials. A systematic comparison between the Roeser–Huber calculations for both rhombohedral and hexagonal representations remains an interesting topic for future research. We note further that the crystal parameters enter directly into the RH formalism; therefore, variations of these parameters parameters inevitably influence the calculated values of $\Delta_{(0)}$ and T_c(calc). As an example, Wang et al. [35] employed $a = 0.4305$ nm and $c = 1.3121$ nm, corresponding to deviations of 0.6% and 3.4%, respectively. Such differences in the structural parameters provide an indirect estimate of the potential uncertainty in the methodology or the resulting predic-

tion of T_c(calc). Thus, all crystallographic data employed here stem from the work of Emery et al. [2].

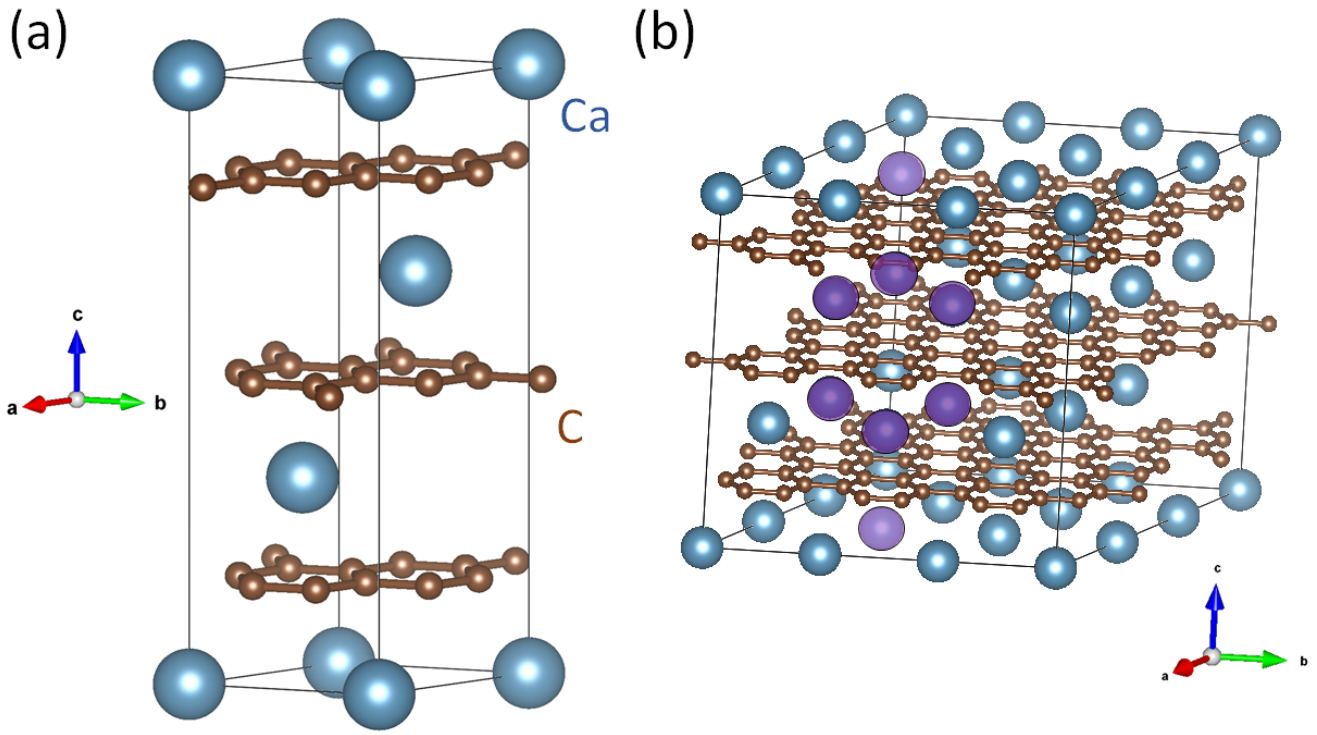

Figure 2. Crystal structure of CaC_6. (**a**) The hexagonal representation of the rhombohedral unit cell of CaC_6, (**b**) view of a $3 \times 3 \times 1$ supercell, which reveals the staggering of the equilateral Ca triangles within the crystal structure. One possible superconducting path between the two light violet Ca atoms via two equilateral Ca triangles (marked dark violet) is shown (see also Figure 5), and a second path can be recognized on the right of it.

The structure of CaC_6 consists of different layers, with C and Ca layers arranged alternatingly (see Figure 2a,b). The carbon atoms in the C layers form hexagons. The Ca atoms form equilateral triangles within the layers with the distance $d_{\mathrm{Ca-Ca}} = a = 0.4333$ mn, but are staggered, which leads to three different arrangements called α, β and γ layers. The resulting stacking order is $A\alpha A\beta A\gamma A\alpha A\beta A\gamma \ldots$ The $3 \times 3 \times 1$ supercell presented in Figure 2b gives a view of the carbon planes and the main Ca layer located in between and provides a better impression of the environments along the possible and not-possible superconducting paths carried by the Ca atoms. One possible symmetric path is indicated by the Ca atoms marked in violet, showing also the equilateral triangles. More details of this will be discussed in Figure 5 below.

3.2. Electronic Configuration of Ca and C

Pure carbon is not superconducting in its intrinsic form; superconductivity appears only when additional charge carriers are introduced through doping, as discussed in Ref. [36]. In contrast, calcium becomes a superconductor under high pressure [37,38]. The T_c can reach up to 29 K under gigabar pressure (phase Ca-VII, 210 GPa). Stoichiometric considerations show that each Ca atom with the electron configuration $[Ar]4s^2$ donates two electrons to the C atoms, thus Ca reaches the configuration Ca^{2+}. In consequence, each C atom in the unit cell receives 1/3 electron.

Superconductivity within the graphite layers themselves would correspond to a two-dimensional (2D) superconducting state, implying the possible presence of more than one superconducting gap. To assume such superconductivity in the graphite sheets, one would have to define a characteristic length within the layer, analogous to the doping distance in high-T_c superconductors [39,40]. However, as no structural defects or distortions within the graphite layers of GICs have been reported, it is natural to consider the intercalant (Ca) atom spacing as this characteristic length. Using this distance, $a = 0.42825$ nm and setting $M_L = 2m_e$, leads to unphysically high values for T_c and the related energy, $\Delta_{(0)}$. Performing the inverse calculation—deriving the characteristic length x from the experimentally observed T_c via Equation (1)—yields $x = 7.433$ nm. Such a large distance could only arise from a corrugated or wavy graphene layer within the CaC_6 lattice, a feature not observed experimentally. Therefore, it is more plausible that superconductivity originates from the Ca sublattice, with the C atoms contributing indirectly through phonon-mediated interactions.

Takada [41–43] performed quantitative first-principles calculations of T_c for both CaC_6 and YbC_6. In these studies, a parameter f was introduced to represent the fractional contribution of the 2D graphite π band and the 3D band by the intercalant orbitals and graphite interlayer states. T_c was evaluated as function of f. The results showed that doubling the atomic number Z of the intercalant element enhances T_c by one order of magnitude, while tripling the effective mass, m^*, has a similar effect. In particular, $m^* = 2.8m_e$ is required to obtain T_c close to the experimentally obtained values. These calculations provide valuable guidance for increasing T_c in GIC systems. Importantly, we see in the RH formalism that an increase in the number of *near* atoms along the superconducting path directly influences the mass parameter, M_L.

Further insight comes from experimental measurements of the superconducting state of CaC_6. Gonnelli et al. [12] used point-contact Andreev reflection (PCAR) spectroscopy to determine the pairing energy, $\Delta(0)$ in *a*,*b*- and *c*-directions. The results obtained there are as follows: $\Delta_{ab}(0) = 1.36 \pm 0.35$ meV ($2\Delta_{ab}(0)/(k_B T_c) = 2.83$) and $\Delta_c(0) = 1.70 \pm 0.19$ meV ($2\Delta_c(0)/(k_B T_c) = 3.54$). Measurements using scanning tunneling microscopy and spectroscopy (STM/STS) reported in [11,13,14] provided the following results: $\Delta_{ab}(0) = 2.1$–2.4 meV (average 2.3 ± 0.19 meV; ($2\Delta_{ab}(0)/(k_B T_c) = 3.54$) [13]; $\Delta_c(0) = 1.6 \pm 0.2$ meV [14]; and $\Delta_c(0) = 1.79 \pm 0.08$ meV ($2\Delta_c(0)/(k_B T_c) = 3.6 \pm 0.2$) [11]. These experimental results point to conventional s-wave superconductivity. The recorded spectra and their temperature dependence are consistent with a single, isotropic BCS gap of approximately 1.6 meV, with no evidence of two-band superconductivity such as that found in MgB_2. This observation further supports the conclusion that superconductivity in CaC_6 is primarily carried by the Ca atoms, with the carbon network acting as a phonon-coupled mediator.

3.3. Remarks to the Measurements of T_c

It is important to note that the RH formalism requires the mean field transition temperature, T_c^{MF}, for the comparison with the calculated values. T_c^{MF} is also a key parameter in fluctuation conductivity analyses [44–46]. Experimentally, T_c^{MF} is best determined from the temperature derivative of the resistivity, $d\rho/dT$, as the peak position of this curve. In contrast, T_c is often derived from 50% of the normal-state resistance, which does not necessarily coincide with T_c^{MF}, particularly in materials exhibiting a broadened or two-step superconducting transition.

For CaC_6, most available data come from magnetic susceptibility measurements rather than resistivity measurements. According to Refs. [20,47], the T_c determined by magnetic susceptibility corresponds to T_c^{onset} of the resistance measurements, which is somewhat larger as T_c^{MF}. However, as the measured superconducting transitions are very sharp with $\Delta T_c \sim 0.1$–0.2 K, there is no need to count for this difference. The situation changes

under applied pressure, where the superconducting transitions become visibly broadened. In these cases, T_c^{MF} is significantly lower than T_c^{onset}, reflecting enhanced inhomogenity and fluctuation effects.

Jobilong et al. [48] reported resistivity measurements on CaC_6 in both the in-plane and out-of-plane configurations. From fits to the normal-state data above T_c, they obtained a Debye temperature, $\Theta_D = 175$ K and the electron-phonon coupling constant λ of 1. These results place CaC_6 in the intermediate to strong coupling regime. Such parameters are highly relevant for assessing the position of CaC_6 in the Uemura plot [25], which in turn is essential for determining appropriate values of the scaling factor η and the effective mass, M_L, used in the RH formalism.

3.4. Determination of the Superconducting Paths

In this section, we now determine the superconducting paths within the unit cell. The essential criterion according to the RH formalism is the symmetry of the path along which the superconducting charge carriers can propagate. To visualize the possible superconducting paths and the atoms that may interact with the Cooper pairs, the simple unit cell as shown in Figure 2a is often not sufficient. Instead, supercells must be constructed, for example, a $3 \times 3 \times 1$ supercell as presented in Figure 2b or a $1 \times 1 \times 2$ supercell as shown in Figure 3. Using these, three symmetric paths can be identified, two located within the (*a*,*b*)-plane and one along the *c*-axis.

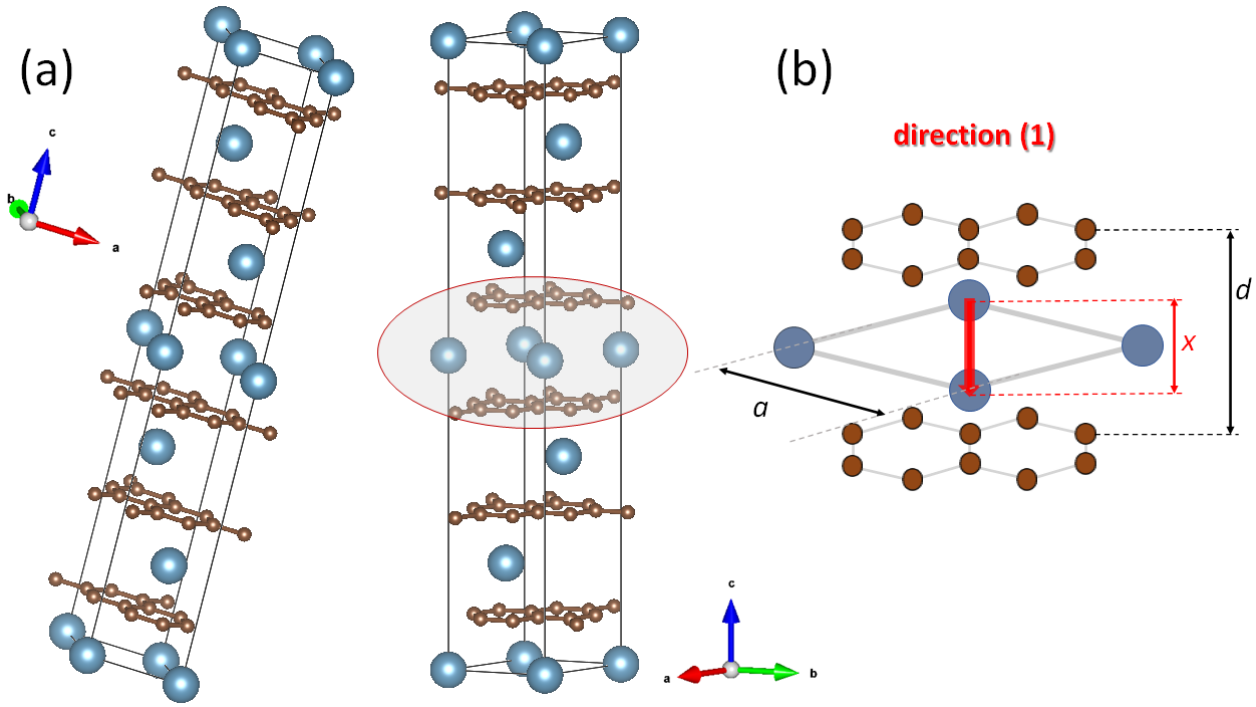

Figure 3. (**a**) Two views of a $1 \times 1 \times 2$ supercell; in the right graph, the section of the equilateral triangles is encircled. (**b**) A schematic drawing of the superconducting charge carrier path in direction (1) within the (*a*,*b*)-plane as indicated by a red arrow and its surroundings for better counting the passed, near atoms.

Direction (1): Along the edge of the unit cell via the Ca atoms (see Figure 3).
Direction (2): Along the face diagonal via the Ca atoms (see Figure 4).
Direction (3): Along the *c*-axis via the Ca atoms (see Figure 5).

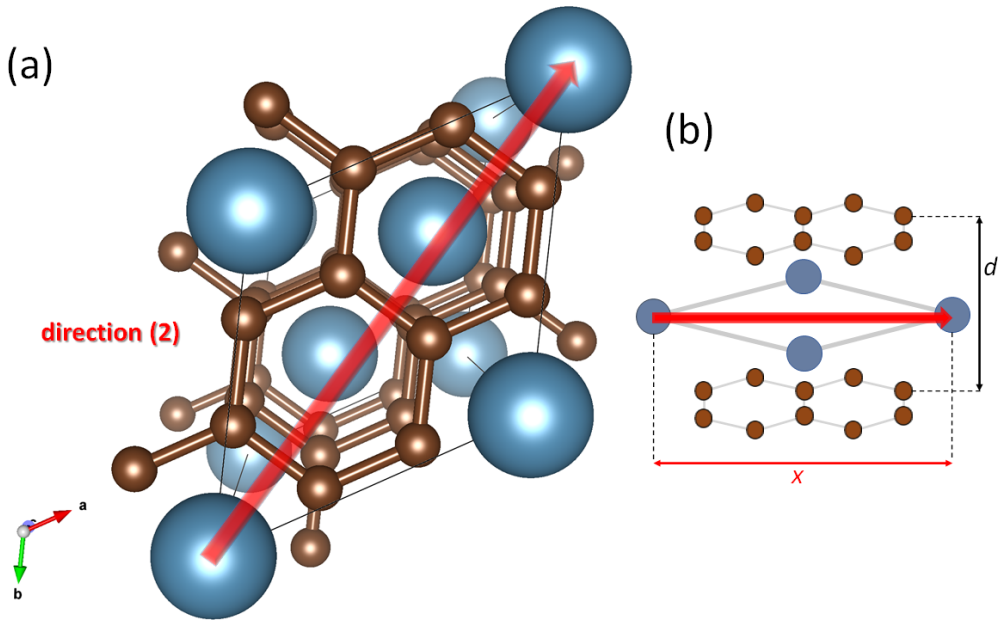

Figure 4. The superconducting charge carrier path in direction (2) in the (*a*,*b*)-plane, (**a**) view in *c*-axis direction. (**b**) is a schematical drawing for better counting the passed, near atoms.

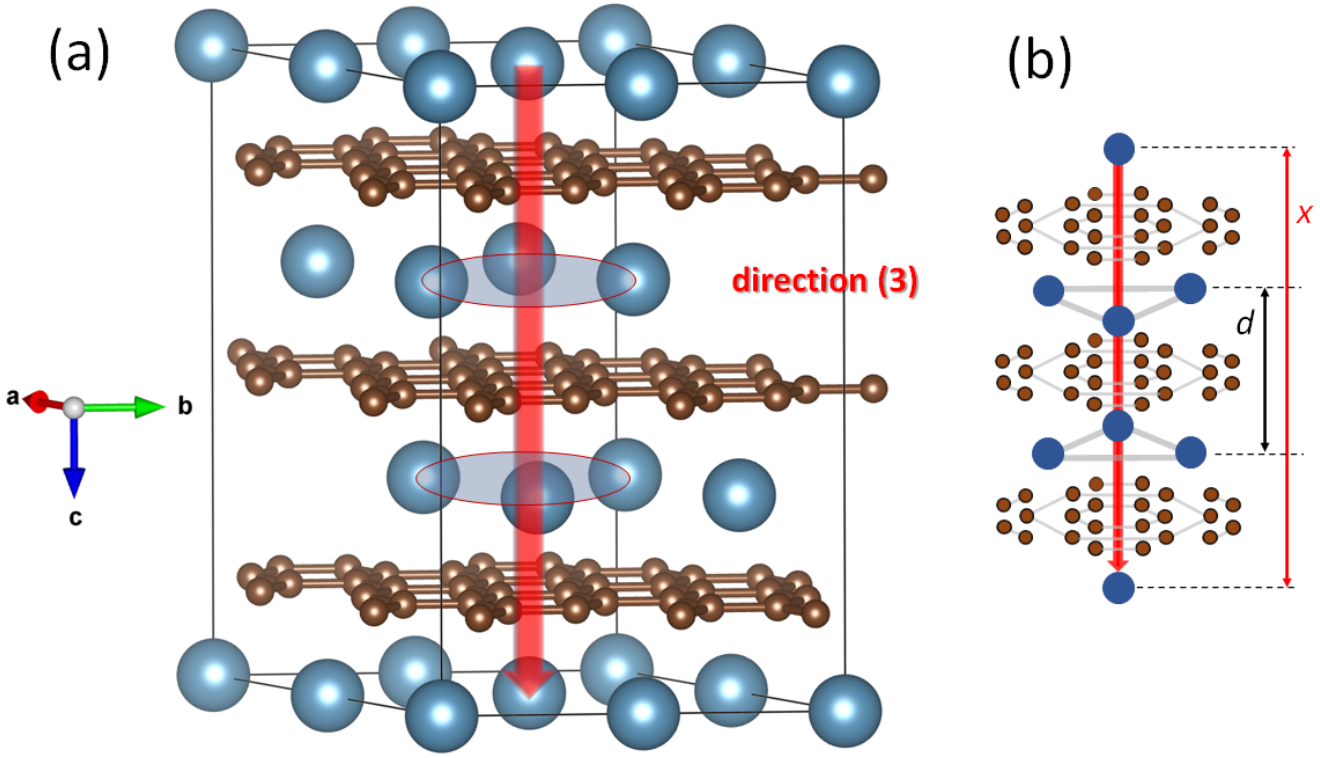

Figure 5. The superconducting charge carrier path in direction (3). (**a**) presents a 2 × 2 × 1 supercell with the rings indicated for the Ca atomtriangles, and (**b**) is a schematical drawing for better counting the passed, near atoms.

For direction (1), the in-plane edge path, the distance between the two Ca atoms is $x = a = 0.433$ nm. The Cooper pairs pass two Ca atoms and four C atoms. The distance between the path and the near Ca atoms is calculated as

$$l_{\mathrm{Ca}} = \frac{\sqrt{3}}{2}a = 0.375 \text{ nm} \ (\frac{l_{\mathrm{Ca}}}{x} = 0.866 \text{ nm}). \tag{2}$$

The distance of the path to the 4 near C atoms is given by

$$l_{\mathrm{C}} = \frac{1}{2}d = 0.226\ \mathrm{nm}\ \ (\frac{l_{\mathrm{C}}}{x} = 0.522\ \mathrm{nm}). \tag{3}$$

Also of interest are the distances between the planes, which contain the passed atoms, to the Ca atom marking the begin of the path. These can be calculated as

$$h_{\mathrm{E1}} = \quad d_{\mathrm{CC}} = 0.144\ \mathrm{nm}\ \ (\mathrm{C-atoms}) \tag{4}$$

$$h_{\mathrm{E2}} = \frac{3}{2}\, d_{\mathrm{CC}} = 0.216\ \mathrm{nm}\ \ (\mathrm{Ca-atoms}). \tag{5}$$

In direction (2), the in-plane diagonal path (see Figure 4a,b) counts as follows: The distance between the two Ca atoms is $x = \sqrt{3}a = 0.750$ nm. On this path, there are 2 Ca atoms and 20 C atoms. The distance to the two Ca atoms can be calculated as

$$l_{\mathrm{Ca}} = \frac{1}{2}a = 0.2165\ \mathrm{nm}\ \ (\frac{l_{\mathrm{Ca}}}{x} = 0.289\ \mathrm{nm}). \tag{6}$$

The distance to the nearest 12 C atoms is given by

$$l_{\mathrm{C1}} = \sqrt{\frac{1}{4}d^2 + \frac{1}{4}d_{\mathrm{CC}}^2} = 0.237\ \mathrm{nm}\ \ (\frac{l_{\mathrm{C1}}}{x} = 0.316\ \mathrm{nm}). \tag{7}$$

and the distance to the next 8 C atoms is

$$l_{\mathrm{C2}} = \sqrt{\frac{1}{4}d^2 + d_{\mathrm{CC}}^2} = 0.268\ \mathrm{nm}\ \ (\frac{l_{\mathrm{C2}}}{x} = 0.357\ \mathrm{nm}). \tag{8}$$

The distances to the planes where the passed, near atoms are located are calculated as

$$h_{\mathrm{E1}} = \frac{\sqrt{3}}{2}\ \ d_{\mathrm{CC}} = 0.125\ \mathrm{nm}\ \ (\mathrm{C-atoms}) \tag{9}$$

$$h_{\mathrm{E2}} = \sqrt{3}\ \ d_{\mathrm{CC}} = 0.250\ \mathrm{nm}\ \ (\mathrm{C-atoms}) \tag{10}$$

$$h_{\mathrm{E3}} = 3\frac{\sqrt{3}}{2}\, d_{\mathrm{CC}} = 0.375\ \mathrm{nm}\ \ (\mathrm{C-andCa-atoms}) \tag{11}$$

In direction (3), the out-of-plane path (c-axis path, see Figure 5a,b), the distance between the two Ca atoms is $x = c = 3d = 1.3572$ nm. On this path, the Cooper pairs will two rings consisting of three Ca atoms and three layers of C atoms. The symmetry of this configuration is ensured by the triangular Ca arrangement, whose centers define the superconducting path. Furthermore, the overlapping electron clouds of the Ca atoms can be viewed as a full ring. In each of the C layers are 6 atoms with the closest distance, 6 atoms with a larger distance, and 12 atoms with the largest distance. To visualize all this, it is useful to schematically redraw the situation as shown in Figure 6b.

The distance of the path to the Ca atoms is given by

$$l_{\mathrm{Ca}} = \frac{\sqrt{3}}{3}a = 0.25\ \mathrm{nm}\ \ (\frac{l_{\mathrm{Ca}}}{x} = 0.184\ \mathrm{nm}). \tag{12}$$

The distance to the ($3 \times 6 = 18$) closest C atoms is calculated to

$$l_{\mathrm{C1}} = d_{\mathrm{CC}} = 0.1444\ \mathrm{nm}\ \ (\frac{l_{\mathrm{C1}}}{x} = 0.106\ \mathrm{nm}). \tag{13}$$

The distance to the ($3 \times 6 = 18$) C atoms with the larger distance is

$$l_{C2} = 2d_{CC} = 0.2888 \text{ nm} \ \ (\frac{l_{C3}}{x} = 0.213 \text{ nm}). \tag{14}$$

The distance to the ($3 \times 12 = 36$) atoms with the largest distance is given by

$$l_{C3} = \sqrt{\left(\frac{3\sqrt{3}}{2}d_{CC}\right)^2 + \left(\frac{1}{2}d_{CC}\right)^2} = \sqrt{7}\, d_{CC} = 0.382 \text{ nm} \ \ (\frac{l_{C3}}{x} = 0.281 \text{ nm}). \tag{15}$$

Finally, the distance between the layers with the passed atoms to the starting point (Ca atom) is given by

$$h_{E1} = \frac{1}{2}d = 0.226 \text{ nm} \ \ (\text{C} - \text{atoms}) \tag{16}$$

$$h_{E2} = \ \ d = 0.452 \text{ nm} \ \ (\text{Ca} - \text{atoms}) \tag{17}$$

$$h_{E3} = \frac{3}{2}d = 0.679 \text{ nm} \ \ (\text{C} - \text{atoms}) \tag{18}$$

Criterion for Near Atoms

To determine whether a passed atom is close enough to influence the Cooper pairs on the superconducting path, we adopt a modified proximity criterion. In earlier RH studies (e.g., for La [21]), atoms were counted as "near" when $l_{calc}/x \leq 0.5$. For more complex lattices, a standing sinusoidal wave model for the Cooper pair and de Broglie wavelength provides a more refined condition:

$$l_{calc} \leq \frac{1}{2}x \sin\left(\frac{h_E}{x}\pi\right) \tag{19}$$

and

$$0 \leq h_E \leq \frac{\pi}{2} \ \ , \tag{20}$$

with x denoting the half of the de Broglie wavelength of the Cooper pairs and h_E the distance between the plane including the atoms to the starting atom. The second relationship given in Equation (20) is the proportion between h_E and l.

Table 1 summarizes the resulting values for $l_{Ca,C}$ and l_{calc} Equation (19). From direct comparison, direction (1) includes no near atoms, and direction (2), involves 14 near atoms (that is, 4 carbon atoms being near enough in layer (2), and as this plane exists twice, these have to be counted double, i.e., $4 + 4 = 8$ atoms. In layer (3), there are 2 close Ca atoms and 4 C atoms, making the complete number of atoms for this direction $8 + 2 + 4 = 14$ atoms). Direction (3) includes 52 atoms. The superconducting charge carriers have to pass all three layers, so we have now 12 carbon atoms in layer (1), which must be counted twice, so 24 atoms. In layer (2), there are three close Ca atoms, which must be counted twice, making six atoms. Finally, in layer (3) there are 22 near atoms. So, the final sum of all atoms being near to the superconducting path counts to $24 + 6 + 22 = 52$ atoms.

Table 1 summarizes all these considerations from the crystal structure, together with the maximal allowed distances, l_{calc}, obtained from Equation (19).

The second way to count the near, passed atoms is given by Equation (20). Here, all atoms having a value < 1 should not be close enough. This procedure yields the following results: In direction (1), there are no near atoms. For direction (2), we have $2 + 4 = 6$ atoms, and in direction (3), there are $12 + 6 + 22 = 40$ atoms. All values, which fulfill the two relations, are given in Table 1 using blue color.

Table 1. Calculation of the required distances.

Direction	Layer	Number of Atoms/Type	h_E [nm]	h_E/x	$l_{Ca,C}$ [nm]	l_{calc} [nm]	$h_E/l_{Ca,C}$
(1)	2 × E1	2 C	0.144	0.333	0.226	0.187	0.637
	2 × E2	2 Ca	0.216	0.499	0.375	0.217	0.576
(2)	2 × E1	4 C	0.125	0.167	0.237	0.187	0.527
	2 × E2	4 C	0.25	0.333	0.268	0.325	0.933
	1 × E3	2 Ca	0.375	0.5	0.217	0.375	1.732
		4 C	0.375	0.5	0.237	0.375	1.583
(3)	2 × E1	6 C	0.2262	0.1667	0.144	0.344	1.571
		6 C			0.289	0.344	0.783
		10 C			0.382	0.344	0.592
	2 × E2	3 Ca	0.452	0.353	0.184	0.616	2.459
	1 × E3	6 C	0.679	0.5	0.144	0.688	4.713
		6 C			0.289	0.688	2.348
		10 C			0.382	0.688	1.776

3.5. Steps to Obtain the T_c and Discussion

Now, we have all the ingredients to proceed with the calculation of the transition temperature, T_c.

The values for T_c(calc) in Table 2 give the T_c values for each individual direction according to the number of near, passed atoms. This enables to judge which configuration is the best suited one. We also see that for directions (1) and (2), there is no single value close to measured T_c of about 11.5 K. However, if one combines the values written in blue with 0 passed near atoms (in the calculation, N_{atoms} is set equal 1) and direction (2) with 14 near atoms, one obtains $T_{c(0)ab} = 11.43$ K and the corresponding $\Delta_{(0)ab} = 3.095$ meV, which closely reproduces experiment. This situation is not so far off as both directions are located in the same crystal plane and differ only by an angle of 30°.

In direction (3), the *c*-axis direction, the blue marked data yield a T_c of 10.68 K ($\Delta_{(0)c} = 2.89$ meV, which is very close to the measured data, and even more, the calculated lowest energy levels (about equal to the superconducting gaps) reveal the same difference between the (*ab*)- and (*c*)-directions as the measured data [12].

An interesting trend emerges from Table 2 and Figure 6: The data for T_c(calc) and $\Delta_{(0)}$ increase systematically with the number of the near, passed atoms. This trend may help to explain the enhanced superconductivity in more complex systems such as carbon-based compounds (diamond, C_{60}, HOPG, graphene) [36] and high-pressure metal hydrides [49–51], where dense atomic environments lead to elevated T_c values even for simple s-wave pairing.

CaC_6 under pressure was studied in Refs. [15–17] and the recorded superconducting transition temperatures were found to raise linearly up to 15.1 K at 7.5 GPa [16]. DFT calculations of this situation were performed by Wang et al. [35]. Commonly, the application of high pressures reduces the unit cell volume, and accordingly the *a*- and *c*-directions, leading to a reduction of the characteristic length, x. Using the reported compressibilities by Gauzzi et al. [17] $da/dP = -0.0038$ Å/GPa and $dc/dP = -0.081$ Å/GPa, the RH formalism yields 13.75 K and 16.21 K for out-of-plane at 7.5 GPa applied pressure, in excellent agreement with experiment. Moreover, compression likely increases the number of near atoms, further enhancing T_c. For example, assuming 72 near atoms along the *c*-axis (direction (3)) leads to 14.78 K, while 4 near atoms in direction (1) yield $T_c = 17.48$ K.

To validate the RH approach further, T_c was calculated as well for the YbC_6 GIC compound, which crystallizes in the hexagonal space group P63/mmc (194), but the possible

symmetric paths for the superconducting electrons are quite similar to CaC_6. Taking the electronic configuration of Yb as Yb^{2+} leads to $\Delta_{ab(0)} = 1.65$ meV and $T_{c(0)ab} = 6.09$ K and $\Delta_{c(0)} = 1.47$ meV and $T_{c(0)c} = 5.43$ K, consistent with the experiment (for more details, see the Supplementary Materials). These results confirm the predictive strength of the RH formalism for complex materials and demonstrate its ability to reproduce experimental superconducting parameters in layered compounds such as CaC_6 and YbC_6.

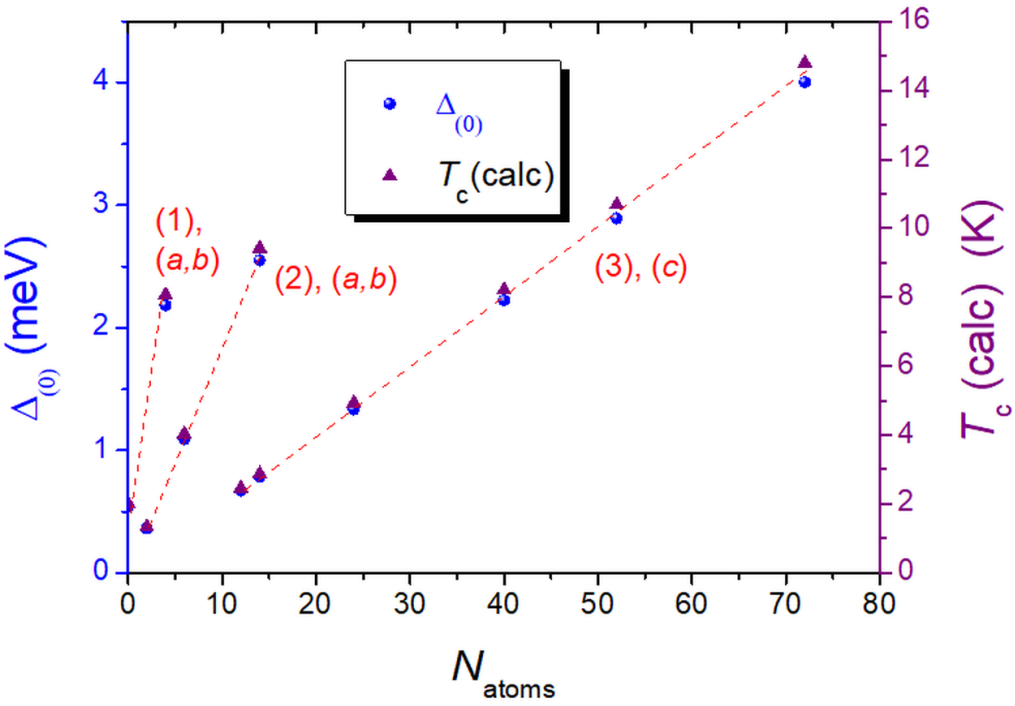

Figure 6. Plot of the number of the near, passed atoms N_A versus $\Delta_{(0)}$ (left axis) and T_c(calc); see also the data presented in Table 2. The dashed red lines show the relation for each of the superconducting paths (1), (2) and (3).

Table 2. Calculation of T_c.

Direction	x [nm]	N_L	N_{atoms}	M_L [ηm_e]	$\Delta_{(0)}$ [meV]	T_c(calc) [K]
(1), (a,b)	0.433	2	0 *	2	0.546	2.02
			4	0.5	2.185	8.07
(2), (a,b)	0.750	2	2	1	0.364	1.34
			6	0.3333	1.092	4.03
			14	0.1429	2.549	9.41
(3), (c)	1.357	2	12	0.1667	0.671	2.46
			14	0.1429	0.783	2.87
			24	0.0833	1.334	4.93
			40	0.05	2.224	8.21
			52	0.0385	2.891	10.68
			72	0.0278	4.003	14.78

* In case of $N_{atoms} = 0$, the calculation is performed with $N_{atoms} = 1$.

Altogether, the results obtained demonstrate that the RH formalism can be effectively employed in the search for graphite intercalation compounds (GICs) with even higher superconducting transition temperatures. Knowledge of the superconducting pathways can significantly aid this search, eliminating the need for time-consuming calculations. Following the work of Takada [41–43], a practical approach is provided that suggests a

route toward higher T_c values: (i) doubling Z, which enhances T_c by roughly one order of magnitude, and (ii) tripling m^*, which similarly enhances T_c by one order. Candidate structures mentioned by Takada include, for instance, compounds like MgC_2 and BeC_2. These systems are especially interesting as the number of C atoms in the unit cell is reduced as compared to CaC_6, but there may be more than one superconducting path within one unit cell, which leads to $n_2 > 1$, thus increasing effectively our parameter η. Takada further proposes the synthesis of three-element GICs that form a heavy three-dimensional electron system by introducing heavy atoms into a light-atom polar-crystal environment. Such potential structures could be systematically examined in the future using the RH formalism.

4. Conclusions

In conclusion, we have carried out a calculation of the superconducting transition temperature (T_c) for the graphite intercalation compounds CaC_6 and YbC_6 within the framework of the RH formalism. To enable these calculations, the criteria defining the passed and near atoms in the crystal structure were refined. This refinement allows for a quantitative reproduction of the experimentally observed T_c values for both compounds, including CaC_6 under applied pressure. The present findings suggest that the RH formalism can provide a reliable description of superconductivity in complex crystal structures.

Supplementary Materials: The following supporting information can be downloaded at https://www.mdpi.com/article/10.3390/met15121367/s1, Figure S1: Crystal structure of YbC_6. (a) standard configuration, (b) view along the *c*-direction. Figure S2: The superconducting charge carrier path in direction (1) indicated by red arrows. Figure S3: The superconducting charge carrier path in direction (2) indicated by red arrows. Figure S4: The superconducting charge carrier path in direction (3). (a) presents the $2 \times 2 \times 1$ unit cell, and (b) is a schematical drawing for better counting the passed, near atoms. Table S1: Calculation of T_c. References [52–54] are cited in the supplementary materials.

Author Contributions: Conceptualization, M.R.K.; Formal Analysis, A.K.-V. and M.R.K.; Investigation, A.K.-V. and M.R.K.; Visualization, A.K.-V. and M.R.K.; Writing—Original Draft Preparation, M.R.K.; Writing—Review and Editing, A.K.-V. and M.R.K. All authors have read and agreed to the published version of the manuscript.

Funding: The work in Saarbrücken was partly subsided by the SUPERFOAM international project funded by ANR and DFG under the references ANR-17-CE05-0030 and DFG-ANR Ko2323-10, which is gratefully acknowledged.

Institutional Review Board Statement: Not applicable.

Informed Consent Statement: Not applicable.

Data Availability Statement: The original contributions presented in this study are included in the article/Supplementary Materials. Further inquiries can be directed to the corresponding author.

Conflicts of Interest: Authors Michael R. Koblischka and Anjela Koblischka-Veneva are the co-founders of the consulting company Supra Saar. The authors declare that they have no conflicts of interest.

References

1. Weller, T.E.; Ellerby, M.; Saxena, S.S.; Smith, R.P.; Skipper, N.T. Superconductivity in the intercalated graphite compounds C_6Yb and C_6Ca. *Nat. Phys.* **2005**, *1*, 39–41. [CrossRef]
2. Emery, N.; Hérold, C.; Lagrange, P. Structural study and crystal chemistry of the first stage calcium graphite intercalation compound. *J. Solid State Chem.* **2005**, *178*, 2947–2952. [CrossRef]
3. Emery, N.; Hérold, C.; d'Astuto, M.; Garcia, V.; Bellin, C.; Marêché, J.F.; Lagrange, P.; Loupias, G. Superconductivity of Bulk CaC_6. *Phys. Rev. Lett.* **2005**, *95*, 087003. [CrossRef] [PubMed]
4. Emery, N.; Hérold, C.; Marêché, J.-F.; Lagrange, P. Synthesis and superconducting properties of CaC_6. *Sci. Technol. Adv. Mater.* **2008**, *9*, 044102. [CrossRef]

5. Kim, J.S.; Boeri, L.; O'Brien, J.R.; Razavi, F.S.; Kremer, R.K. Superconductivity in Heavy Alkaline-Earth Intercalated Graphites. *Phys. Rev. Lett.* **2007**, *99*, 027001. [CrossRef]
6. Kadowaki, K.; Nabemoto, T.; Yamamoto, T. Synthesis and superconducting properties of graphite compounds intercalated with Ca:C_6Ca. *Phys. C* **2007**, *460–462*, 152–153. [CrossRef]
7. Smith, R.P.; Weller, T.E.; Howard, C.A.; Dean, M.P.M.; Rahnejat, K.C.; Saxena, S.S.; Ellerby, M. Superconductivity in graphite intercalation compounds. *Phys. C* **2015**, *514*, 50–58. [CrossRef]
8. Csányi, G.; Littlewood, P.B.; Nevidomskyy, A.H.; Pikard, C.P.; Simons, B.D. The role of the interlayer state in the electronic structure of superconducting graphite intercalated compounds. *Nat. Phys.* **2005**, *1*, 42–45. [CrossRef]
9. Mazin, I.I. Intercalant-Driven Superconductivity in YbC_6 and CaC_6. *Phys. Rev. Lett.* **2005**, *95*, 227001. [CrossRef]
10. Calandra, M.; Mauri, F. Theoretical Explanation of Superconductivity in C_6Ca. *Phys. Rev. Lett.* **2005**, *95*, 237002. [CrossRef] [PubMed]
11. Lamura, G.; Aurino, M.; Cifariello, G.; Gennaro, E.D.; Andreone, A.; Emery, N.; Hérold, C.; Marêché, J.-F.; Lagrange, P. Experimental Evidence of s-Wave Superconductivity in Bulk CaC_6. *Phys. Rev. Lett.* **2006**, *96*, 107008. [CrossRef]
12. Gonnelli, R.S.; Daghero, D.; Delaude, D.; Tortello, M.; Ummarino, G.A.; Stepanov, V.A.; Kim, J.S.; Kremer, R.K.; Sanna, A.; Profeta, G.; et al. Evidence for Gap Anisotropy in CaC_6 from Directional Point-Contact Spectroscopy. *Phys. Rev. Lett.* **2008**, *100*, 207004. [CrossRef] [PubMed]
13. Kurter, C.; Ozyuzer, L.; Mazur, D.; Zasadzinski, J.F.; Rosenmann, D.; Claus, H.; Hinks, D.G.; Gray, K.E. Large energy gaps in CaC_6 from tunneling spectroscopy: Possible evidence of strong-coupling superconductivity. *Phys. Rev. B* **2006**, *76*, 220502R. [CrossRef]
14. Bergeal, N.; Dubost, V.; Noat, Y.; Sacks, W.; Roditchev, D.; Emery, N.; Hérold, C.; Marêché, J.F.; Lagrange, P.; Loupias, G. Scanning tunneling spectroscopy on the novel superconductor CaC_6. *Phys. Rev. Lett.* **2006**, *97*, 077003. [CrossRef] [PubMed]
15. Kim, J.S.; Boeri, L.; Kremer, R.K.; Razavi, F.S. Effect of pressure on superconducting Ca atomintercalated graphite CaC_6. *Phys. Rev. B* **2006**, *74*, 214513. [CrossRef]
16. Gauzzi, A.; Takashima, S.; Takeshita, N.; Terakura, C.; Takagi, H.; Emery, N.; Hérold, C.; Lagrange, P.; Loupias, G. Enhancement of Superconductivity and Evidence of Structural Instability in Intercalated Graphite CaC_6 under High Pressure. *Phys. Rev. Lett.* **2007**, *98*, 067002. [CrossRef]
17. Gauzzi, A.; Bendiab, N.; d'Astuto, M.; Canny, B.; Calandra, M.; Mauri, F.; Loupias, G.; Emery, N.; Hérold, C.; Lagrange, P.; et al. Maximum T_c at the verge of a simultaneous order-disorder and lattice-softening transition in superconducting CaC_6. *Phys. Rev. B* **2008**, *78*, 064506. [CrossRef]
18. Roeser, H.P.; Haslam, D.T.; Lopez, J.S.; Stepper, M.; von Schoenermark, M.F.; Huber, F.M.; Nikoghosyan, A.S. Correlation between transition temperature and crystal structure of niobium, vanadium, tantalum and mercury superconductors. *Acta Astronaut.* **2010**, *67*, 1333–1336. [CrossRef]
19. Stepper, M. Calculation of the Transition Temperature of Two-Component-Superconductors. IRS 08-S23. Master's Thesis, Institute of Space Systems, University of Stuttgart, Stuttgart, Germany, 2008. (In German)
20. Koblischka, M.R.; Roth, S.; Koblischka-Veneva, A.; Karwoth, T.; Wiederhold, A.; Zeng, X.L.; Fasoulas, S.; Murakami, M. Relation between Crystal Structure and Transition Temperature of Superconducting Metals and Alloys. *Metals* **2020**, *10*, 158. [CrossRef]
21. Koblischka, M.R.; Koblischka-Veneva, A. Calculation of T_c of Superconducting Elements with the Roeser–Huber Formalism. *Metals* **2022**, *12*, 337. [CrossRef]
22. Buckel, W.; Kleiner, R. *Supraleitung. Grundlagen und Anwendungen*, 7th ed.; Wiley-VCH: Weinheim, Germany, 2013. (In German)
23. Koblischka, M.R.; Koblischka-Veneva, A. Review of Moiré superconductivity and application of the Roeser-Huber formula. *Superconductivity* **2024**, *9*, 100073. [CrossRef]
24. Rohlf, J.W. *Modern Physics from α to* Z^0; Wiley: New York, NY, USA, 1994.
25. Uemura, Y.J.; Le, L.P.; Luke, G.M.; Sternlieb, B.J.; Wu, W.D.; Brewer, J.H.; Riseman, T.M.; Seaman, C.L.; Maple, M.B.; Ishikawa, M.; et al. Basic Similarities among Cuprate, Bismuthate, Organic, Chevrel-Phase, and Heavy-Fermion Superconductors Shown by Penetration Depth Measurements. *Phys. Rev. Lett.* **1991**, *66*, 2665–2668. [CrossRef] [PubMed]
26. ICDD. *ICDD PDF Data Base*; ICDD: Newtown Square, PA, USA. Available online: https://www.icdd.com/pdfsearch/ (accessed on 15 March 2025).
27. Materials Project Database V2019.05. Available online: https://materialsproject.org/ (accessed on 15 March 2025).
28. Crystallography Open Database (COD). Available online: https://www.crystallography.net/cod/index.php (accessed on 15 March 2025).
29. Stanev, V.; Oses, C.; Kusne, A.G.; Rodriguez, E.; Paglione, J.; Curtarolo, S.; Takeuchi, I. Machine learning modeling of superconducting critical temperature. *NPJ Comput. Mater.* **2018**, *4*, 29. [CrossRef]
30. Lee, D.; You, D.; Lee, D.; Li, X.; Kim, S. Machine-Learning-Guided Prediction Models of Critical Temperature of Cuprates. *J. Phys. Chem. Lett.* **2021**, *12*, 6211–6217. [CrossRef]
31. Konno, T.; Kurokawa, H.; Nabeshima, F.; Sakishita, Y.; Ogawa, R.; Hosako, I.; Maeda, A. Deep learning model for finding new superconductors. *Phys. Rev. B* **2021**, *103*, 014509. [CrossRef]

32. Ghosh, K.J.B.; Kais, S.; Herschbach, D.R. Dimensional interpolation for metallic hydrogen. *Phys. Chem. Chem. Phys.* **2021**, *23*, 7841–7848. [CrossRef]
33. CrystalMaker Software Ltd.: Begbroke, Oxfordshire, UK. Available online: https://crystalmaker.com/ (accessed on 15 March 2025).
34. Momma, K.; Izumi, F. VESTA 3 for three-dimnsional visualization of crystal, volumetric and morphology data. *J. Appl. Crystallogr.* **2011**, *44*, 1272–1276. [CrossRef]
35. Wang, B.; Bianconi, A.; Mackinnon, I.D.R.; Alarco, J.A. Superlattice Symmetries Reveal Electronic Topological Transition in CaC_6 with Pressure. *Crystals* **2024**, *14*, 554. [CrossRef]
36. Zheng, X.H.; Zheng, J.X. Room-temperature superconductivity in carbons—A mini review. *Phys. Lett. A* **2024**, *525*, 129936. [CrossRef]
37. Yabuuchi, T.; Matsuoka, T.; Nakamoto, Y.; Shimizu, K. Superconductivity of Ca Exceeding 25 K at Megabar Pressures. *J. Phys. Soc. Jpn.* **2006**, *75*, 083703. [CrossRef]
38. Szcześniak, R.; Durajski, A.P. Superconductivity of calcium in phase VI. *Phys. C* **2012**, *472*, 15–20. [CrossRef]
39. Roeser, H.P.; Hetfleisch, F.; Huber, F.M.; Stepper, M.; von Schoenermark, M.F.; Moritz, A.; Nikoghosyan, A.S. A link between critical transition temperature and the structure of superconducting $YBa_2Cu_3O_{7-\delta}$. *Acta Astronaut.* **2008**, *62*, 733–736. [CrossRef]
40. Roeser, H.P.; Hetfleisch, F.; Huber, F.M.; von Schoenermark, M.F.; Stepper, M.; Moritz, A.; Nikoghosyan, A.S. Correlation between oxygen excess density and critical temperature in superconducting Bi-2201, Bi-2212 and Bi-2223. *Acta Astronaut.* **2008**, *63*, 1372–1375. [CrossRef]
41. Takada, Y. Unified Model for Superconductivity in Graphite Intercalation Compounds: Prediction of Optimum T_c and Suggestion for Its Realization. *J. Phys. Soc. Jpn.* **2009**, *78*, 013703. [CrossRef]
42. Takada, Y. Mechanism of Superconductivity in Graphite Intercalation Compounds Including CaC_6. *J. Supercond. Nov. Magn.* **2009**, *22*, 89–92. [CrossRef]
43. Takada, Y. Mechanism of Superconductivity in Graphite-Alkali Metal Intercalation Compounds. *J. Phys. Soc. Jpn.* **1982**, *51*, 63–72. [CrossRef]
44. Mori, N.; Wilson, J.A.; Ozaki, H. Fluctuation conductivity in the 110-K phase of Ni-doped (Bi,Pb)-Sr-Ca-Cu-O superconductors. *Phys. Rev. B* **1992**, *45*, 10633–10638. [CrossRef]
45. Larkin, A.; Varlamov, A. *Fluctuation Phenomena in Superconductors*; Oxford University Press: Oxford, UK, 2005.
46. Koblischka, M.R.; Koblischka-Veneva, A.; Zeng, X.L.; Hannachi, E.; Slimani, Y. Microstructure and Fluctuation-Induced Conductivity Analysis of $Bi_2Sr_2CaCu_2O_{8+\delta}$ (Bi-2212) Nanowire Fabrics. *Crystals* **2020**, *10*, 986. [CrossRef]
47. Koblischka, M.R. *Magnetic Properties of High-T_c Superconductors*; Alpha Science International: Oxford, UK, 2009.
48. Jobiliong, E.; Zhou, H.D.; Janik, J.A.; Jo, Y.-J.; Balicas, L.; Brooks, J.S.; Wiebe, C.R. Anisotropic superconductivity in bulk CaC_6. *Phys. Rev. B* **2007**, *76*, 052511. [CrossRef]
49. Semenok, D.V.; Kruglov, I.A.; Savkin, I.A.; Kvashnin, A.G.; Oganov, A.R. On Distribution of Superconductivity in Metal Hydrides. *Curr. Opin. Solid State Mat. Sci.* **2020**, *24*, 100808. [CrossRef]
50. Meier, T.; Laniel, D.; Trybel, F. Direct hydrogen quantification in high-pressure metal hydrides. *Matter Radiat. Extrem.* **2023**, *8*, 018401. [CrossRef]
51. Sun, Y.; Zhong, X.; Liu, H.; Ma, Y. Clathrate metal superhydrides under high-pressure conditions: Enroute to room-temperature superconductivity. *Natl. Sci. Rev.* **2024**, *11*, nwad270. [CrossRef] [PubMed]
52. Ellerby, M.; Weller, T.E.; Saxena, S.S.; Smith, R.P.; Skipper, N.T. Superconductivity at elevated temperatures in C_6Yb and C_6Ca. *Physica B* **2006**, *378–380*, 536–639. [CrossRef]
53. Sutherland, M.; Doiron-Leyraud, N.; Taillefer, L.; Weller, T.; Ellerby, M.; Saxena, S.S. Bulk Evidence for Single-Gap s-Wave Superconductivity in the Intercalated Graphite Superconductor C_6Yb. *Phys. Rev. Lett.* **2007**, *98*, 067003. [CrossRef] [PubMed]
54. Springer Materials. Available online: https://materials.springer.com/isp/crystallographic/docs/sd_0530003 (accessed on 15 March 2025).